PHOTOGRAPH THIS SHEET

AD-A995 398

DTIC ACCESSION NUMBER

LEVEL

INVENTORY 1

CLOUD CHEMISTRY OF FALLOUT FORMATION

FINAL REPORT

DOCUMENT IDENTIFICATION

DISTRIBUTION STATEMENT A
Approved for public release;
Distribution Unlimited

DISTRIBUTION STATEMENT

ACCESSION FOR
NTIS GRA&I ☒
DTIC TAB ☐
UNANNOUNCED ☐
JUSTIFICATION

BY
DISTRIBUTION /
AVAILABILITY CODES

DIST	AVAIL AND/OR SPECIAL
A-1	23

DISTRIBUTION STAMP

UNANNOUNCED

DTIC
ELECTE
MAR 0 4 1986
S D
D

DATE ACCESSIONED

DATE RETURNED

[illegible] 003

DATE RECEIVED IN DTIC

REGISTERED OR CERTIFIED NO.

PHOTOGRAPH THIS SHEET AND RETURN TO DTIC-DDAC

DTIC FORM 70A DEC 83

DOCUMENT PROCESSING SHEET

PREVIOUS EDITION MAY BE USED UNTIL STOCK IS EXHAUSTED.

Gulf General Atomic
Incorporated

GA-8472
OCD Work No. 3111A T.O. No. 3110(67)

CLOUD CHEMISTRY OF FALLOUT FORMATION

FINAL REPORT

by

J. H. Norman, P. Winchell,
and H. G. Staley

Prepared for
Office of Civil Defense
Office of the Secretary of the Army
Department of Defense, 20310
under
Contract N0022867C1675
through the
Technical Management Office,
U.S. Naval Radiological Defense Laboratory,
San Francisco, California 94135

January 31, 1968

Gulf General Atomic
Incorporated
P.O. Box 608, San Diego, California 92112

GA-8472
OCD Work No. 3111A T.O. No. 3110(67)

CLOUD CHEMISTRY OF FALLOUT FORMATION

FINAL REPORT

by

J. H. Norman, P. Winchell,
and H. G. Staley

Performed for
Office of Civil Defense
Office of the Secretary of the Army
Department of Defense, 20310
under
Contract N0022867C1675
through the
Technical Management Office,
U.S. Naval Radiological Defense Laboratory,
San Francisco, California 94135

Gulf General Atomic Project 6035 January 31, 1968

488

CONTENTS

FIGURES

FIGURES (continued)

TABLES

CLOUD CHEMISTRY OF FALLOUT FORMATION

FINAL REPORT

by

J. H. Norman, P. Winchell, and H. G. Staley

Gulf General Atomic Incorporated Report GA-8472

January 31, 1968

SUMMARY

Calculations of fission-product distribution in fallout for the Small Boy event have been made using a condensed-state diffusion-controlled fission-product absorption model. The properties of calculated fission-product inventories in particles with size distribution supplied correlated reasonably well with properties of actual Small Boy fallout inventories. An evaluation of these inventories using the DELFIC fission-product distribution system is being made.

Henry's law has been demonstrated to be applicable to the system cesium/O_2/CaO-Al_2O_3-SiO_2 eutectic. The derived Henry's law constants have been shown to be independent of the oxygen pressure ($1 \geq P_{O_2}$ (atm) $> \sim 10^{-4}$) and of water pressure ($0.03 \geq P_{H_2O}$ (atm) $> \sim 10^{-4}$).

The diffusion coefficients of cesium in Small Boy soil have been measured. These measurements provide some justification for employing diffusion coefficients of fission products in CaO-Al_2O_3-SiO_2 eutectic for the Small Boy calculations. Studies of diffusion coefficients of fission products created in situ in silicate matrices have been initiated.

Some preliminary fission-product leaching studies have been made. A program for studying the leaching of recoiled fission products from silicates is outlined.

Mass spectrometric Knudsen cell studies have demonstrated the apparent importance of such species as $CeO_2(g)$, $PrO_2(g)$, $NdO_2(g)$, and $TcO_3(g)$ to fallout formation processes.

INTRODUCTION

During the course of the fallout formation studies program this year, progress has been made in understanding nuclear cloud chemistry and in applying this understanding and its effects to the distribution and behavior of fission products in fallout. While most of the studies at Gulf General Atomic have been directly involved with the measurement of chemical phenomena associated with cloud chemistry, an important portion of the program has been associated with the calculation of the distribution of fission products in fallout for the Small Boy shot and the subsequent analysis of the calculated particle activities. The results presented in this report suggest that the calculated distributions are reasonably realistic; it is felt that in further analysis, now in progress using the DELFIC model, these distributions will also be realistic.

Proving that Henry's law is applicable to the solution of cesium in $CaO\text{-}Al_2O_3\text{-}SiO_2$ eutectic has been one of the results of this program. Transpiration studies have also confirmed the similarity in chemical behavior between cesium and rubidium. However, the exact nature of the equilibria between alkali metal doped silicate and a gas phase is still unknown.

Studies to test the diffusivities of fission products in Small Boy soil were carried out; the application of diffusivities determined in $CaO\text{-}Al_2O_3\text{-}SiO_2$ eutectic in Small Boy calculations was deemed reasonable. Diffusion studies on fission products made <u>in situ</u> from U^{235} dissolved in eutectic $CaO\text{-}Al_2O_3\text{-}SiO_2$ are promising. Some agreement with previous methods has been demonstrated. This method allows the ready study of nuclides such as Xe^{133} and I^{131} and provides a survey method for studying silicates.

Some leaching studies were performed. The major accomplishment in this field has been the establishment of procedures that appear useful in describing leaching of fission products from silicates. It is believed that a description sufficient to asscciate a leaching model with the diffusion-controlled fission product absorption model can be attained, and thus a description of the effects of early cloud chemistry. It is believed that the model output will be very valuable to a long-term damage assessment program.

Mass spectrometric Knudsen cell studies of the stability of the rare-earth dioxides have shown surprisingly high stabilities of some of these oxides, particularly $NdO_2(g)$. Indeed, the existence of gaseous rare-earth dioxides for most of the rare earths might be forecast from these studies. A second M-O bond energy of about 60% of the first M-O bond has been observed for Pr and Nd. The dioxide existence is important in cloud chemistry as these species predominate in the oxidizing atmospheres generally associated with nuclear events.

Knudsen cell studies of rhenium and technetium oxides have been performed mass spectrometrically. A comparison of the stabilities of $M_2O_7(g)$ and $MO_3(g)$ has resulted from this work. The $Tc_2O_7(g)$ stability versus $TcO_3(g)$ stability will prove to be quite useful in the estimation of the behavior of the cloud chemistry of this element.

SMALL BOY CALCULATIONAL STUDIES

As a test of the diffusion-controlled fission product absorption model,[1] calculations for a simulated Small Boy shot have been made. The Small Boy shot is one of the better documented shots detonated over a silicate matrix; in particular, the description of its fallout behavior is extensive. The test of the calculational model consists of evaluating fission-product inventories from 70 mass chains in Small Boy particles. The size fractions, and total weights of these fractions, were supplied by R. Tompkins[2] of the Nuclear Defense Laboratory. This particular data was extracted from input for calculations of fission product distribution in standard DELFIC calculations[3] for Small Boy and is presented in Table 1. The cloud time-temperature history used in the fission-product absorption calculations was taken from this same source but modified to include an early history according to Hillendahl's model.[4] The employed history is presented in Table 2. In making the calculations, Henry's law constants as reported by Norman[5] and measured and estimated diffusion coefficients[6] were employed. The applicability of these diffusion coefficients to the Small Boy calculational study is considered in this report. Fission yields were taken from the fission fraction of the weapon yield and Miller's[7] energetics description. Fission product contents of each particle size fraction and the amount of fission products remaining in the gas phase 9.8 sec after the detonation are available as output of the Korts and Norman[1] calculational system.

An analysis of the calculated fission product inventories in terms of fractionation factors has been attempted for certain fission product isotopes observed particularly in fallout from the Small Boy event. A listing of elements for which experimental fractionation factors may be available is

TABLE 1

SMALL BOY PARTICLE SIZE-WEIGHT FRACTION DESCRIPTION
(Each particle size fraction contains 7.82×10^7 g fallout)

Radius of Particle Size Fraction (cm)	(cm)
0.699400	0.005649
0.057880	0.004907
0.038825	0.004251
0.029201	0.003663
0.023182	0.003134
0.018987	0.002657
0.015867	0.002221
0.013454	0.001819
0.011511	0.001444
0.009917	0.001086
0.008591	0.000728
0.007464	0.000060
0.006493	

TABLE 2

SMALL BOY TIME-TEMPERATURE HISTORY

Time (sec)	Temperature ($^{\circ}$K)
0.6	4000
0.85	3600
1.2	3200
1.6	2900
2.3	2600
3.0	2400
3.6	2200
4.1	2000
4.7	1800
5.3	1600
6.1	1400
7.0	1200
8.2	1000
9.8	800

TABLE 3

FRACTIONATION RATIOS CALCULATED FOR A SIMULATED SMALL BOY SHOT $\left(\frac{C_i}{F_i} \Big/ \frac{C_{95}}{F_{95}}\right)$

Radioactive Nuclide	Particle Radius (cm)			
	0.0292	0.00992	0.00313	0.00109
Sr-89-A	0.0504	0.108	0.245	0.458
-B[a]	0.0793	0.192	0.501	1.16
Sr-90-A	0.128	0.230	0.474	0.860
-B	0.148	0.289	0.650	1.34
Y-91-A	0.243	0.391	0.738	1.29
-B	0.253	0.419	0.820	1.52
Zr-95	1.0	1.0	1.0	1.0
Zr-97	1.05	1.03	0.986	0.933
Mo-99	1.02	1.02	1.00	0.983
Ru-103-A	0.369	0.540	0.913	1.19
-B	0.378	0.569	1.00	1.434
Ru-106-A	0.0936	0.172	0.335	0.443
-B	0.122	0.255	0.585	1.125
Ag-111-A	0.145	0.387	0.916	1.56
-B	0.152	0.407	0.974	1.74
Ag-112-A	0.190	0.500	1.11	1.73
-B	0.192	0.507	1.14	1.80
Sn-123	0.482	0.761	1.02	1.28
Sb-125	0.377	0.686	1.09	1.23
Te-127M	0.247	0.594	1.17	1.48
Te-129M	0.186	0.472	0.976	1.35
I-131-A	0.185	0.465	0.907	1.05
-B	0.198	0.505	1.03	1.38
Te-132-A	0.150	0.377	0.729	0.832
-B	0.169	0.431	0.892	1.28
Cs-136	0.136	0.357	0.898	1.86
Cs-137-A	0.0396	0.105	0.264	0.547
-B	0.0663	0.182	0.499	1.19
Ba-140-A	0.444	0.553	0.810	1.27
-B	0.449	0.567	0.850	1.38
Ce-141	0.678	0.762	0.948	1.29
Pr-143	1.00	1.01	0.991	0.974
Ce-144	1.03	1.02	0.988	0.943
Nd-147	1.04	1.03	0.986	0.932

[a]B values include adsorption of gaseous fission products.

presented in Table 3. These elements are correlated with the value $(C_i F_{95}/C_{95}F_i)$, i.e. $r_{i,95}$, before and after surface adsorption, on assumed spherical particles, of the fission products still gaseous at 800°K, 9.8 sec after detonation, where C_i/C_{95} is the ratio of concentrations in given size fallout particles of the isotope E^i and Zr^{95}, divided by the ratio of total yields of the two isotopes F_i/F_{95}. The values presented in Table 3 correspond to a time when all precursors of the particular isotope have decayed to the isotope E^i or Zr^{95} but only negligible decay of these isotopes has occurred. Behavior of the gaseous fission products may well be more complicated than that of adsorption on the total particle surface area of the nonvolatile products of decay; for instance, some particle-cloud detachment may occur before many volatile precursors decay appreciably. For these types of phenomena, the fallout model could be made more complex to handle the problem. Nevertheless, in the model's present state it is interesting to compare published fractionation ratios with the calculated values for Small Boy. A comparison to Small Boy data of Crocker, Kawahara, and Freiling[8] is presented in Fig. 1. For given nuclides described in this figure, slopes of fractionation plots, i.e., slope of log $r_{i,95}$ vs log $r_{89,95}$, are plotted against the fractionation ratio for the largest of the four particle sizes given in Table 3. These two quantities appear to be closely correlated. The fractionation ratios are described both before and after adsorption of gaseous fission products remaining after 9.8 sec. The circle points include the adsorption while the triangle points include no adsorption after 9.8 sec following detonation.

An attempt to construct fractionation slopes from the calculated fission product sorptions, assuming adsorption after 9.8 sec, is shown in Fig. 2. Some of the fission product distributions give well-defined slopes, while others are better described as curves. The best slope was obtained for a nonlinear fractionation curve. Additionally, whether the curvatures of fractionation plots were essentially zero, positive, or negative

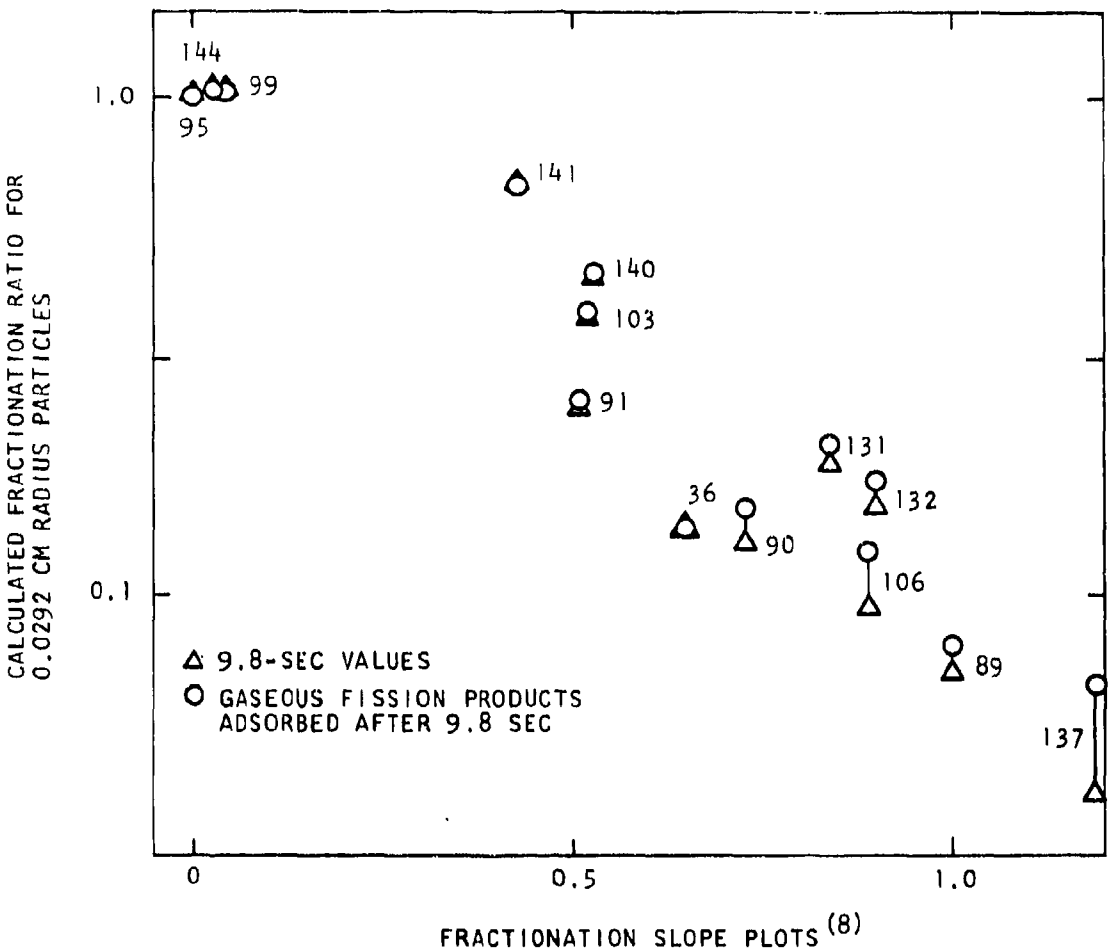

Fig. 1. Correlation of experimental and calculated fractionation in Small Boy

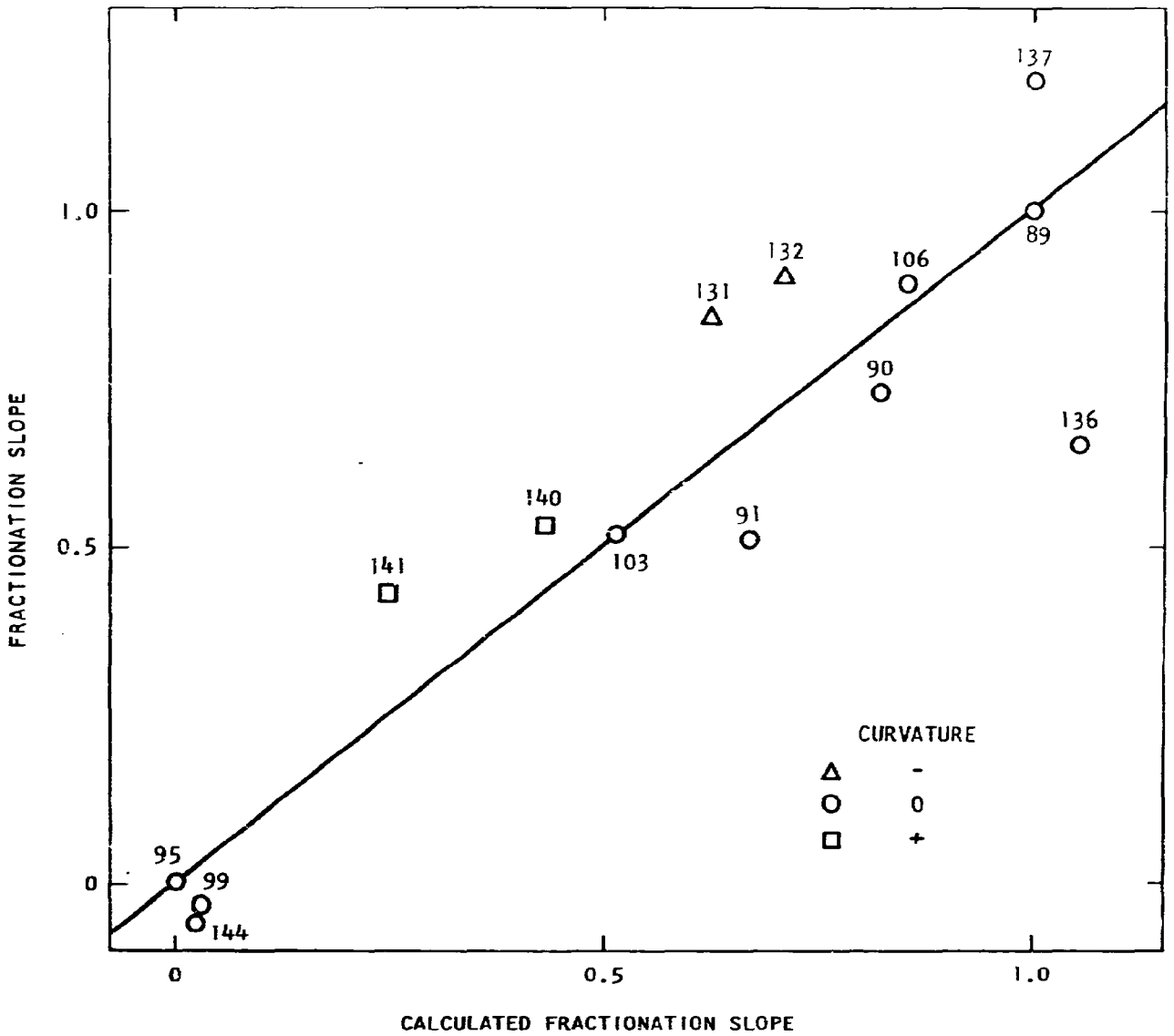

Fig. 2. Correlation of calculated and observed fractionation slopes

was designated by open circles, squares, or triangles, respectively. The agreement is good between calculated and experimental slopes, and since the actual Small Boy experimental data exhibit considerable variance, the agreement with the true situation might even be better.

The two plots in Figs. 1 and 2 suggest agreement between some of the basic properties of calculated and actual Small Boy fallout. Another test that can be made is a comparison between calculated and actual variation of the fractionation ratio of Sr^{89} and Zr^{95} with particle size. Figure 3 is a reproduction of the Crocker, Kawahara, and Freiling[8] experimental data plot with the calculated Small Boy values superimposed. While the calculated fractionation ratios, shown by open circles for adsorption after 9.8 sec and triangles for no adsorption, appear to be somewhat higher for small particles and lower for large particles, there is considerable similarity between the calculated and observed values. There is a trend in the experimental values for the fractionation ratio to become invariant as the particle size increases. The trend might be explained by assuming that these particles do not absorb as much zirconium as the calculational model indicates. Large particles could deplete neighboring gas fields of zirconium and thus not load to the same degree that a small particle in a similar gas field would. A similar problem is noted in the calculational program where large particles do not load strictly on a volume basis. However, this effect is the result of insufficient time for a particle to diffuse zirconium (as an example) to an essentially uniform concentration. This problem may be real and could contribute to a fractionation of zirconium in large particles.

Predictions of the USNRDL radial-distribution model[9] have been added to Fig. 3 by Freiling[10] to compare this model to the diffusion-controlled absorption model. Freiling has also added cloud fractionation ratios as if they pertained to 1 μ particles. The diffusion-controlled model appears to provide a better fit to the data than does the radial-distribution

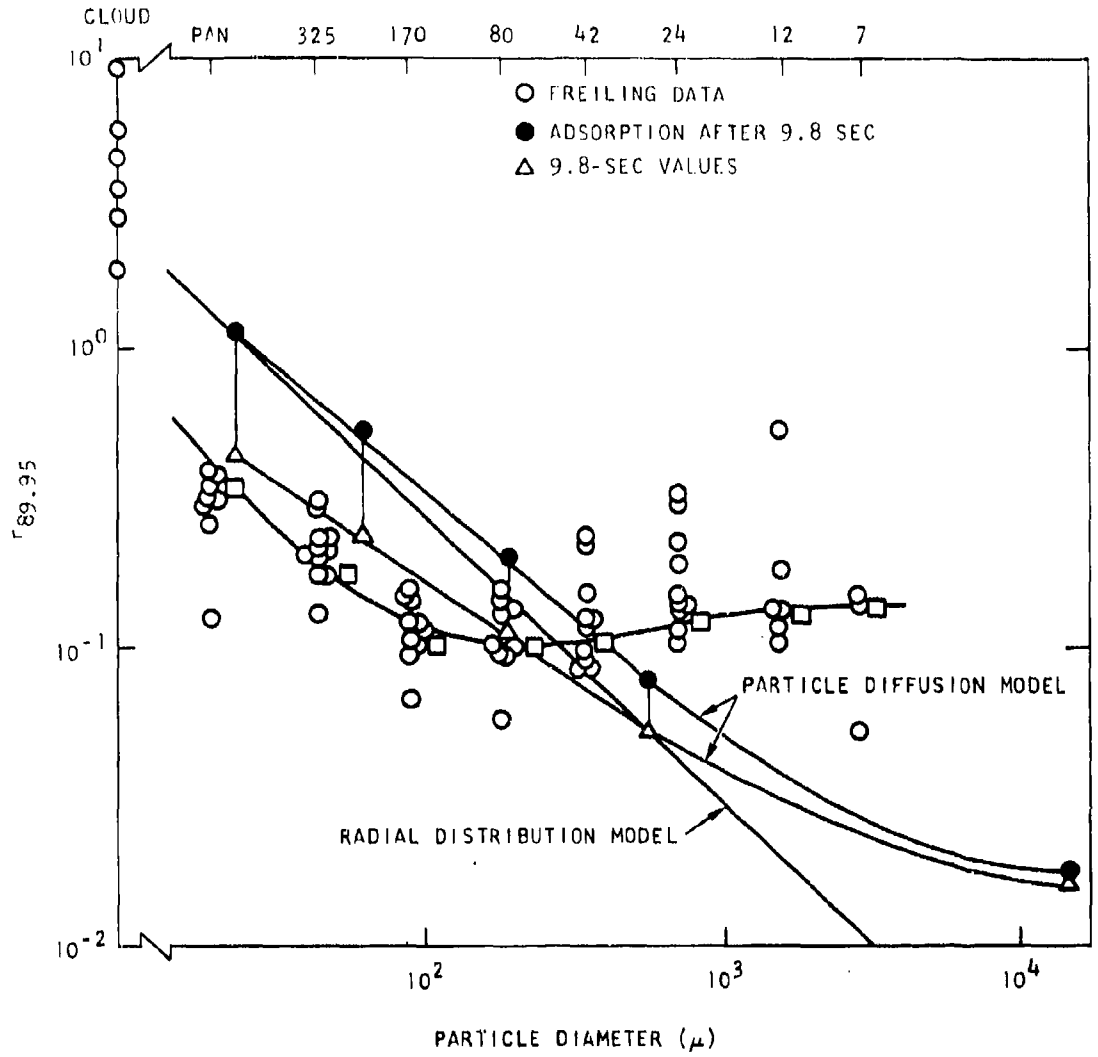

Fig. 3. Effect of particle size on fractionation ratio using actual data[10] and calculated data

model, but the differences are mainly in magnitudes, not in character. Figure 3 suggests that the diffusion model represents an appreciable advance from the radial-distribution model in predicting fission-product distribution in fallout.

These comparison figures are the basis for optimism concerning the calculated distribution of fission products in fallout using the described method. A further test will be the application of the DELFIC particle distribution calculational system by Tompkins using the particle-fission product inventories calculated at Gulf General Atomic.

HENRY'S LAW CONSTANT MEASUREMENT

A formal report[11] covering the Henry's law constant studies performed at Gulf General Atomic during this contract and previous contracts was given to the International Atomic Energy Agency, describing the transpiration method and equipment used in these studies. This report summarizes the positions taken in the IAEA report and extends the information to the end of the contract period.

Using the method of analysis described by Norrman, et al.,[11] cesium transpiration rates at both 1205 to 1208° and 1400°C were measured as a function of dried oxygen carrier-gas flow rate. The cesium sources were two $CaO-Al_2O_3-SiO_2$ 1173°C eutectic composition melts, which initially contained 44 μg Cs/g silicate and 5 μg Cs/g silicate (carrier-free Cs-137). The data at ~1200°C are shown in Figs. 4 and 5. The lines represent the asymptotes for large and small log V of the plotted equation

$$\log \frac{BK\lambda}{P_o AD} = \log \frac{\lambda V}{AD} - \log \left(1 - \exp\left(-\frac{\lambda V}{AD}\right)\right) \qquad (1)$$

as derived by Merten,[12] where K is the transpiration rate (cpm/min), V is the carrier-gas flow rate (cm^3/min), D is the interdiffusion coefficient (cm^2/min), A is the capillary area (cm^2), λ is length (cm), P_o is the equilibrium cesium pressure (atm), and B is a factor that converts cpm to cm^3 atm. The asymptotes are:

as $V \to 0$,

$$\log \frac{BK\lambda}{P_o AD} = 0 , \qquad (2)$$

and as $V \to \infty$,

$$\log \frac{BK\lambda}{P_o AD} = \log \frac{\lambda V}{AD} . \qquad (3)$$

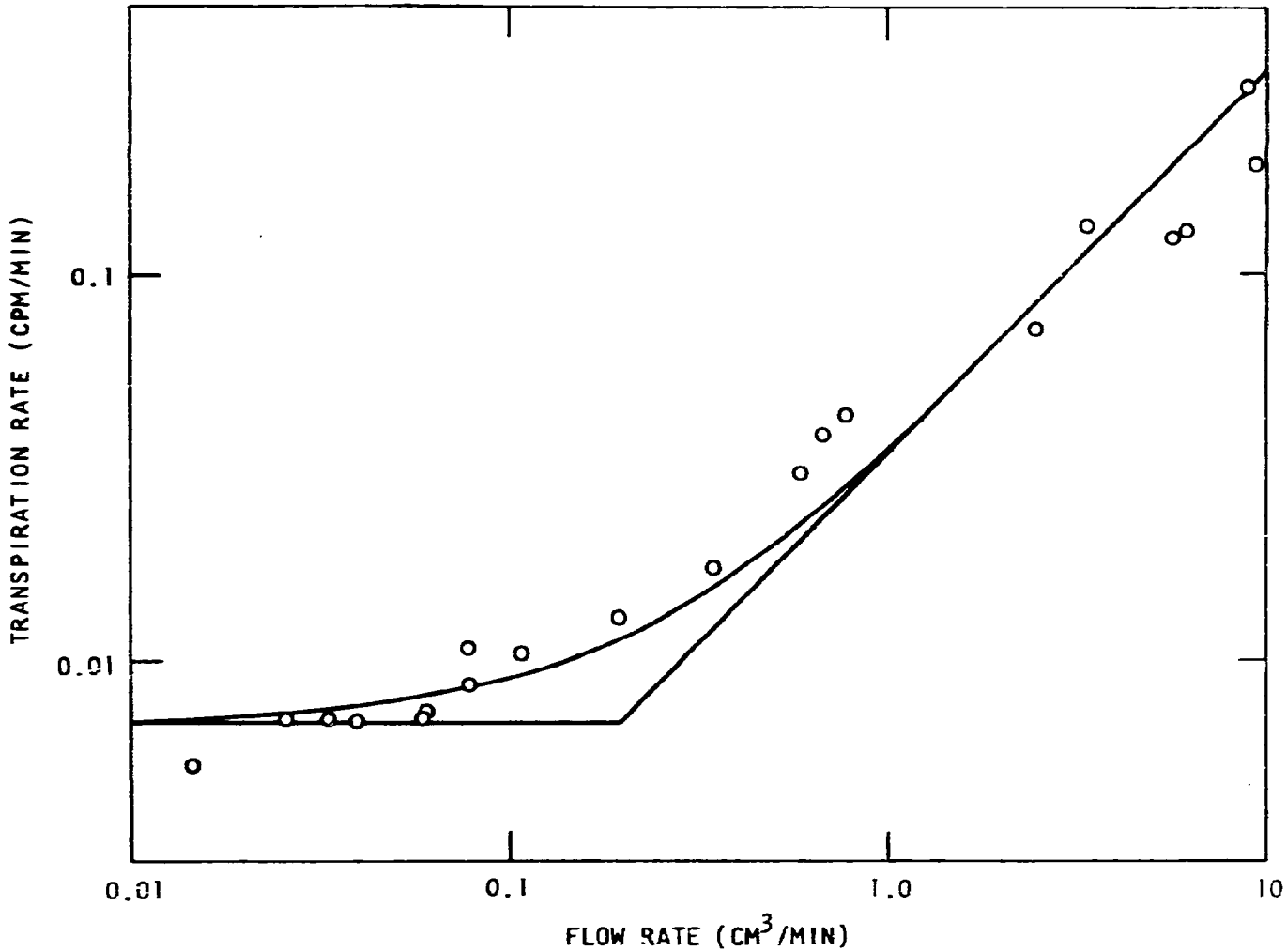

Fig. 4. Study of the transpiration of cesium from the 5 μg Cs/g $CaO-Al_2O_3-SiO_2$ eutectic at 1208°C using O_2 carrier gas

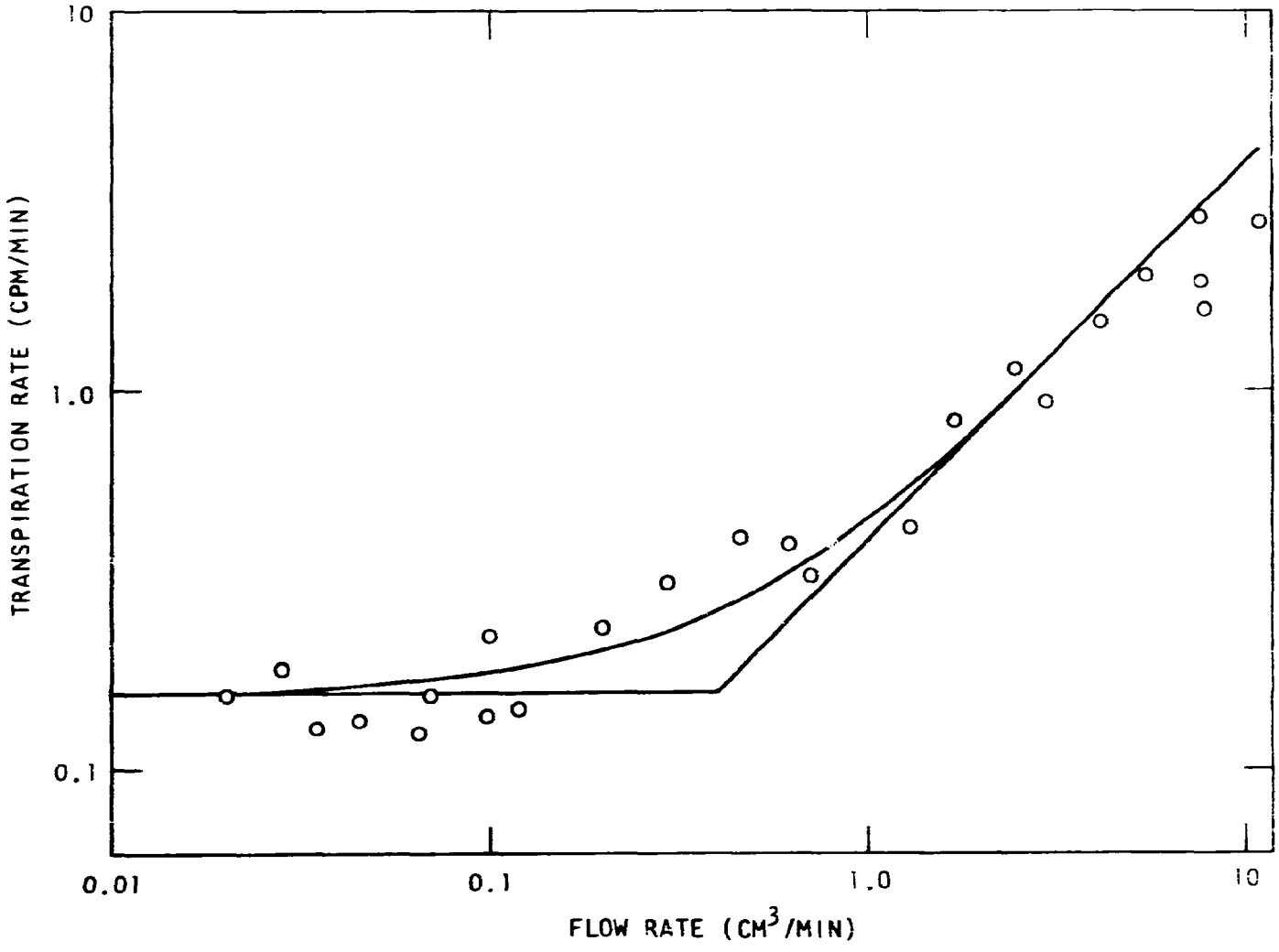

Fig. 5. Study of the transpiration of cesium from the 44 μg Cs/g $CaO-Al_2O_3-SiO_2$ eutectic at 1205°C using O_2 carrier gas

Equation (3) can be reduced to

$$\log \frac{BK}{P_o} = \log V \,, \tag{4}$$

from which experimental K and V data provide a measure of P_o. The studies are made with slightly different capillaries, thus the apparent diffusion coefficients DA/λ differ.

To obtain Henry's law constants from these data, the factor P_o/B (atm cpm/cm^3 atm) must be divided by the specific activity of the melt, S (cpm/g silicate), giving P_o/SB [atm/(cm^3 atm/g silicate)]. Then SB can be related to a cesium concentration C(g Cs/g silicate) through the perfect gas law

$$\frac{SBM}{RT} = C \,, \tag{5}$$

where M is the molecular weight (g/mole) of the cesium gaseous species (assumed monatomic), R is the gas constant (cm^3 atm/^{o}K mole), and T is the temperature (^{o}K). Thus, the Henry's law constant (atm g silicate/g Cs) is

$$H = \frac{P_o}{C} = \frac{P_o RT}{BSM} \,. \tag{6}$$

The particularly noteworthy point is that only the specific activity S of the silicate melt is necessary to derive the Henry's law constant from the experimental data, and not the cesium specific activity itself.

To test Henry's law for this chemical system, the value of the transpiration ratio K/V for the asymptotic line of Eq. (4) was substituted into Eq (6) for P_o/B, obtaining

$$H = \frac{KRT}{VSM} \,. \tag{7}$$

If the transpiration ratio K/V (cpm/cm^3) is plotted on a log-log basis at a constant temperature against the silicate specific activity S (cpm/g silicate), and a unit slope of the line through the data is obtained, the validity of Henry's

law for the system is proved. These ~1200°C data are shown in Fig. 6 and the points provide unit slope within experimental error. Additionally, Fig. 6 shows data taken at 1400°C which also provide confirmation of Henry's law. Note that deviations from the expected unit slope are similar for both sets of data.

Thus, a confirmation of the anticipated chemistry of evaporation of cesium from a dilute cesium solution in the $CaO-Al_2O_3-SiO_2$ melts has been obtained from these data. That is, the degree of cesium association in the melt and the gas phase appear to be the same (i.e., probably one cesium for each gaseous cesium species, and one cesium for each solution species), and the solution is dilute enough so that solute cesium species are not affected by the presence of other solute cesium species. The vaporization reaction can be written as

$$Y + CsX(sol) \rightarrow CsY(gas) + X\,. \qquad (8)$$

Attempts to define X and Y of Eq. (8) have not been too successful. It seems highly probable that CsX(sol) can be considered to be $Cs^+(sol)$. Studies have been made to try to clarify the nature of CsY(gas). Transpiration studies similar to those shown in Figs. 4 and 5 have been made using argon in place of oxygen and water-saturated oxygen in place of oxygen. These tests were designed to find out, first, the oxidation state of the gaseous species,

$$Cs^+(sol) + 1/2\ SiO_3^=(sol) \rightleftarrows Cs(g) + 1/2\ SiO_2(sol) + 1/4\ O_2\,, \qquad (9)$$

and second, whether a volatile hydroxide could be important, thus

$$1/2\ H_2O(g) + Cs^+(sol) + 1/2\ SiO_3^=(sol) \rightleftarrows CsOH(g) + 1/2\ SiO_2(sol). \qquad (10)$$

For the test to be meaningful, the solution chemistry must be essentially unaltered by the change in oxygen pressure or the presence of water vapor. If this is the case, the change in oxygen pressure should affect the cesium Henry's law constant according to Eq. (9) and the water pressure should

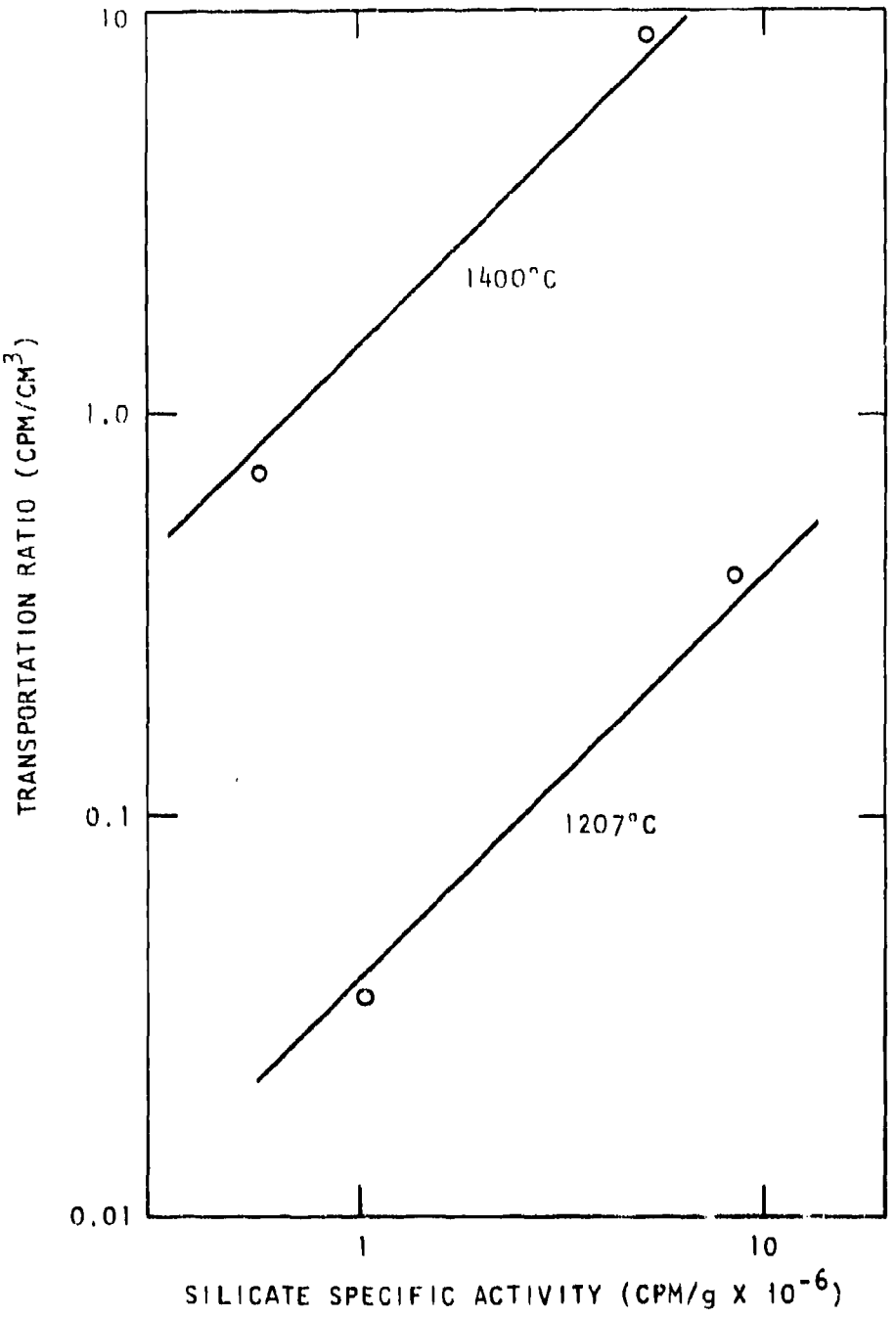

Fig. 6. Confirmation of the applicability of Henry's law to the system cesium dissolved in eutectic $CaO\text{-}Al_2O_3\text{-}SiO_2$

affect the Henry's law constant according to Eq. (10). The experiments using these different gases with both levels of cesium concentration in the melts failed to reveal any sensitivity of Henry's law constant for cesium to these reactant gases, which suggests that Eqs. (9) and (10) may not be applicable. But Eqs. (9) and (10), especially (10), have appeared to be very likely candidates for the condensation processes in fallout formation, in fact, in previous reports mass spectrometric data have been presented that strongly indicate cesium atoms to be the important gaseous species.

The position taken concerning the rubidium, which behaves like cesium,[13] and cesium Henry's law constants, is that these values have been measured under conditions applicable to fallout formation situations. These constants have been demonstrated to be unaffected by certain atmospheric changes. Thus, it is satisfactory to use these measured Henry's law constants in describing this quantity for fallout formation calculations.

In addition to these mechanistic considerations, the cesium Henry's law constants measured during these studies can be compared with some values reported previously.[11] The new 1207°C value is $3.6 \pm 0.8 \times 10^{-5}$ atm/g Cs/g silicate, which is about a factor of four higher than reported previously using another eutectic melt, and the 1400°C value is $1.48 \pm 0.3 \times 10^{-3}$ atm/g Cs/g silicate, which is about a factor of ten higher than obtained with the other melt.

The transpiration data presented in this report, for the case of cesium, (1) agree with the observations of the lack of rubidium sensitivity to studied carrier-gas compositions,[11] (2) confirm the applicability of Henry's law to solutions of cesium in $CaO-Al_2O_3-SiO_2$ eutectic melt, and (3) provide a new measure of the value of the Henry's law constant in this melt.

DIFFUSION OF RADIONUCLIDES IN MOLTEN SILICATES

In this report some of the results of a computation of fallout formation using the Norman[13] calculational model and the Korts and Norman[1] computational program are presented. The computation was done to compare the model with experimental observations for the Small Boy detonation. Part of the input for the program is a set of Arrhenius dependences of diffusion coefficients for the transport of fission products in silicate glasses. The diffusivities include both experimentally determined values and predicted values as have been discussed by Winchell and Norman.[6] However, most of these diffusivities pertain to a particular composition in the CaO-Al_2O_3-SiO_2 ternary system, and it was considered necessary to make at least a cursory comparison of the diffusion of some radionuclide in Nevada soil-based glass with that in the CaO-Al_2O_3-SiO_2 glass. The experiment is described below in detail because the composition and behavior of molten Nevada soil have evidently not been studied.

A sample of Nevada soil obtained from the vicinity of the Small Boy detonation was provided by S. Mikhail of USNRDL. The sample weighed $\sim$ 1 kg and consisted of particles ranging in size from fine dust to small pebbles. This sample was placed on a clean table, randomly mixed, gathered into a cone, and progressively quartered. A final representative sample weighing $\sim$ 20 g was placed in a ceramic assay pot and heated in air for 3 hr at 1000°C to destroy any organic material. The resulting dark red sample was separated into two subsamples: (1) particles of diameter $\gtrsim$ 3 mm and (2) smaller particles. The finer mesh sample was subsampled using a riffle. A resulting sample was placed in a platinum crucible and carefully heated. At about 1300°C the sample frothed, indicating the presence of some volatiles. After heating at that temperature for $\sim$ 1 hr,

the sample was removed from the crucible, powdered in a Diamet mortar, returned to the crucible, and heated for 3 days at 1400°C. The resulting dark glassy material was recovered from the crucible and a representative specimen was mounted in plastic and polished. Microscopic examination of this specimen showed a highly vitreous matrix containing a few small bubbles and some small crystals that may have been quartz. It is estimated that the preparation was at least 95% vitreous in character. The density of this glass was found to be 2.40 g cm^{-3}, which is a typical value for refractory glass. A partial chemical analysis of the glass was made, and in Table 4 the results are compared with the composition of the 1450°K eutectic of the $CaO-Al_2O_3-SiO_2$ ternary system, which is the reference matrix used for diffusion studies in this laboratory. The composition of the eutectic glass differs from that of the Nevada glass principally in the CaO content. This difference is lessened if one considers that Mg behaves similarly to Ca in these glasses and that the equilibrium, $Fe(III) + \bar{e} \rightleftharpoons Fe(II)$, favors ferrous iron in high-temperature acidic silicates, thus increasing the RO content. The differences in silica content of these glasses might become important in the diffusion of glass-forming species such as Sb, but the differences are of second-order importance for the diffusion of the majority of the fission product nuclides. In any case, the initial results obtained for the diffusion of radiocesium in the Nevada matrix are similar to values for the eutectic.

TABLE 4

COMPOSITIONS OF GLASSES IN WEIGHT PERCENT[a]

Glass	SiO_2	CaO	MgO	Al_2O_3	Fe_2O_3	Total
Eutectic	62	23	-	15	-	100
Nevada	68	2	2	18	5	95

[a] The uncertainty is ~1%.

To compare the diffusion of a radionuclide in the Nevada matrix with that in the eutectic matrix, radiocesium was used as the diffusing species. A representative sample of the Nevada glass was divided, mixed with carrier cesium ($\sim$ 1% Cs (NO_3)), melted, divided, and melted and divided again. This sample was then activated in the Gulf General Atomic TRIGA reactor to yield Cs^{134}. Using the plane source technique,[14] experiments were done at 1683°K and 1612°K. The results are compared with those obtained for the diffusion of radiocesium in the eutectic matrix[6] in Table 5.

TABLE 5

COMPARISON OF DIFFUSIVITIES[a] OF RADIOCESIUM IN NEVADA AND EUTECTIC GLASS (cm^2 sec^{-1})

Temperature (°K)	Nevada	Eutectic
1683	4.2×10^{-7}	2.5×10^{-7}
1612	9.9×10^{-8}	7.1×10^{-8}

[a] The uncertainty is $\sim$ 50%.

The data in Table 5 indicate that, with respect to the transport of cesium, the two matrices are essentially equivalent. Again, it is felt that this result can be extrapolated to a majority of the fission product nuclides. It is concluded that, for the purpose of the calculational model, the eutectic matrix is a fair model of the Nevada matrix with respect to diffusion of radionuclides.

The experimental approach to the problem of diffusion in molten silicates has been extended by studying the simultaneous diffusion of several nuclides. Although the technique is still in the developmental stage, it shows considerable promise and a few data have been obtained. The apparatus consists of a water-cooled, high-vacuum, copper jacket with a removable base that supports water-cooled power leads for the furnace and thermocouple lead-throughs. The power leads are brazed to adjustable copper clamps that hold a platinum ribbon resistance element. The element

is indented by use of a special conical tool, and the glass sample is melted into the 70° cone. More glass is then melted onto the sample until the final sample closely approximates the solid figure generated by revolving a 35° sector of a circle about one of its two circle radii. The conical angle is optimized such that, when enough glass is placed in the cone and it just overflows onto the flat portion of the ribbon, the glass is in essentially the form of a spherical sector. This geometry involves the same mathematical model as that for diffusion from a complete sphere into an infinite sink when dealing with a volatile fission product that is insoluble in platinum. The sample temperature has been determined using a Pt-Pt/10% Rh thermocouple attached to the underside of the cone, and using an optical pyrometer to view the platinum in the vicinity of the cone. An "O" ring establishes the vacuum seal between the copper jacket and the furnace base, which can be removed from the jacket by uncoupling the quick-disconnect fitting.

A diffusion experiment is performed by homogeneously doping the glass sample with $\sim 1\%$ UO_2 (U^{235}-enriched), activating the sample in the Gulf General Atomic TRIGA reactor, allowing the fission products to decay for several days, and then annealing the sample for a known period at a known temperature.

A library of lithium-drifted germanium detector gamma-ray photopeak spectra of fission products accumulated at Gulf General Atomic has been compared to experimental spectra as have Ge(Li) detector fission product spectra reported by Gordon, Harvey, and Nakahara.[15] A good correlation has been found among these spectra, so most of the important peaks are well-identified.

On this basis the isotopes in Table 6 seem reasonable to study by the vaporization method.

In the diffusion experiments it has been found necessary to maintain an ambient pressure of a few hundred microns of air instead of a high vacuum to prevent bubble formation, the cause of which is not well understood. After the annealing period, the glass-containing ribbon is situated

TABLE 6

CANDIDATES FOR DIFFUSION STUDIES

Isotope	Important Precursors at Ten Days	Energy (MeV)
Mo^{99}	none	0.181 (0.140)
Tc^{99}	Mo^{99}	0.140
Ru^{103}	none	0.498
I^{131}	$Te^{131}(1)$, $Te^{131}(2)$	0.364
Te^{132}	none	0.233
$Xe^{133}(2)$	I^{133}, $Xe^{133}(1)$	0.081

in a precise position above a lithium-drifted germanium detector, and the gamma-ray spectrum is obtained using a 4096-channel analyzer. This system is capable of resolving peaks separated by only ~ 5 keV. The spectrum can be read out as an oscilloscope photograph, as a printed set of channel and signal values, or as an IBM computer tape containing the channel-signal information. In the last case, a computer program affords peak identifications, integration under peaks, and proper background and decay corrections. The volatile fission products that have been found to be tractable so far with this technique include Xe^{133}, I^{131}, Te^{132}, and, to lesser extents, Mo^{99} and Tc^{99}. An example of the results from this technique is shown in Fig. 7 where the logarithm of the tellurium diffusivity in the 1450°K eutectic is plotted against the reciprocal absolute temperature. These data are described by the equation,

$$\log_{10} D = 3.24 - 14600\ T^{-1}\ , \qquad (11)$$

where D is in $cm^2 sec^{-1}$, T is in °K, and the coefficients were found by the method of least squares with unit weighing. This result agrees well with data obtained using an earlier vaporization technique.[6]

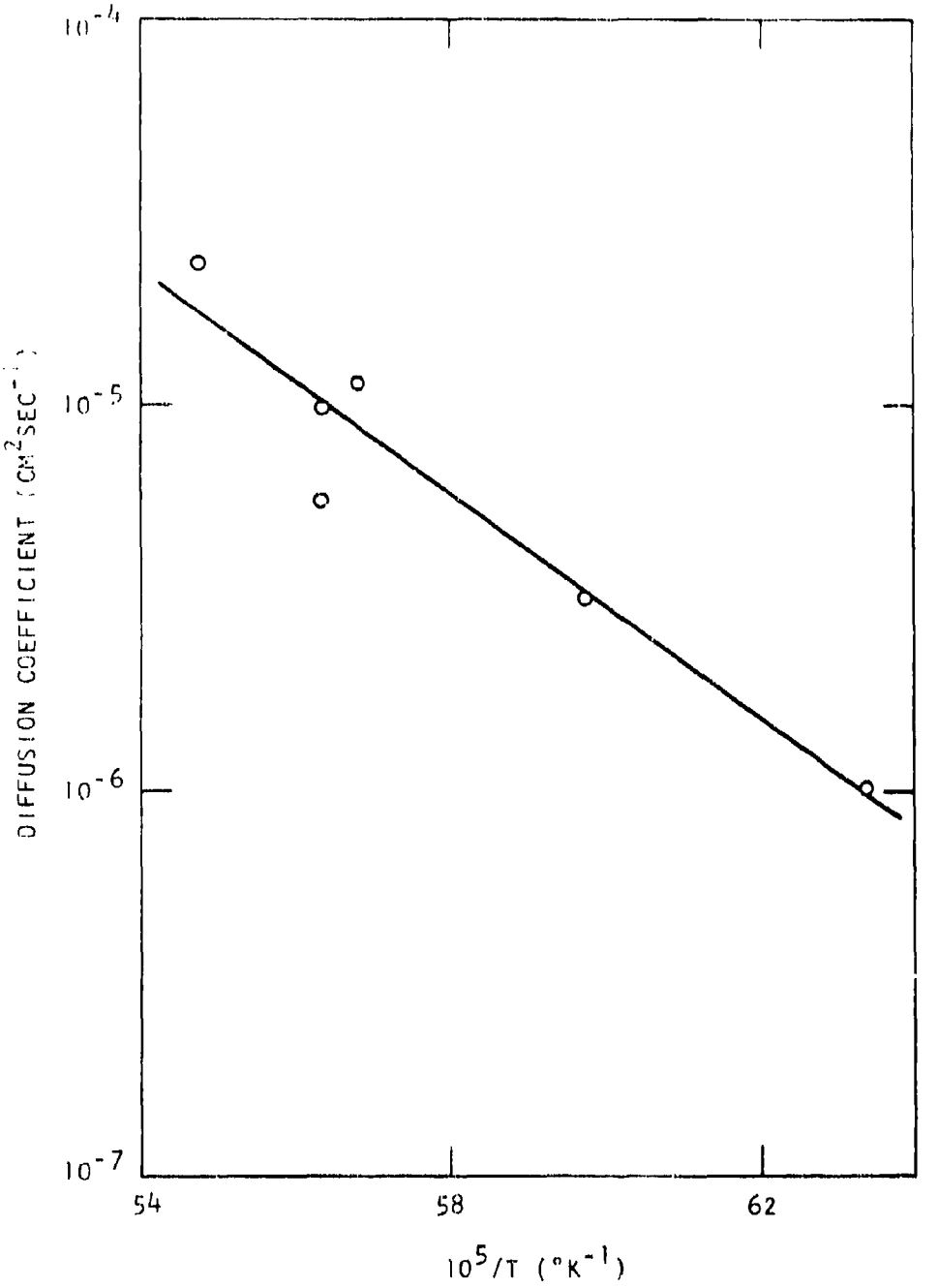

Fig. 7. Diffusion coefficients for the transport of fission product Te-132 in the 1450°K eutectic matrix as measured by the new vaporization technique

The chief merit of the present technique is that it affords the study of the simultaneous transport of several nuclides including those difficult to study otherwise. The method appears to be particularly worthwhile as a means of surveying different kinds of soil.

LEACHING STUDIES

The biological availability of radionuclides from the leaching of silicate fallout particles is an important consideration in the overall problem of fallout. The mechanism of leaching should be understood to the extent that calculations of fission product leaching from particles with concentration gradients may be made. In the previous final report,[13] data for the leaching of iodine from a high-refractory glass were reported. The results indicated that the leaching mechanism was that of desorption. The data reported in this section show that the leaching of sodium from a less refractory glass can be explained by a diffusion-controlled mechanism.

The matrix used for this study was purchased from the National Bureau of Standards in the form of glass spheres (Standard Reference Material 1019). The composition of this glass is similar to that of window glass. The sample was screened using a set of standard sieves and four subsamples were chosen. These samples are described in Table 7.

TABLE 7

GLASS SAMPLES USED FOR LEACHING STUDIES

Sample	Diameter (mm)	Number of Particles
A	2.59 - 2.36	32
B	2.36 - 1.65	39
C	1.65 - 1.17	261
D	1.17 - 0.89	530

Prior to weighing, the samples were inspected for foreign material and briefly washed with distilled water and dried. Irregular shaped or inhomogeneous particles were discarded. After weighing, the samples were

irradiated with neutrons in the Gulf General Atomic TRIGA reactor for 1/2 hr at 250 kW. A multichannel gamma analysis to 2 MeV showed peaks at 0.51, 1.37, and 1.73 MeV, which can be attributed to activated Na (pair production, primary γ, double escape from 2.75 γ) in the glass. The samples were placed in double-thickness Whatman No. 44 filter papers that were held in funnels equipped for aliquoting from the tip. Colorado River tap water with a pH of $\sim$ 8.2 was used as the leachant. Periodically, 10 ml of leachant was added to the glass samples after draining the previous aliquot, which was integrally gamma-counted from 0.4 to 2.0 MeV. Leaching was done at room temperature without agitation. The pH of the leachant remained constant throughout the leaching periods. The overall leaching period was $\sim$ 30 hr.

The results are shown in Fig. 8 where the total amount of activity leached per particle is plotted as a function of the square root of the time. Referring to this figure, it is seen that samples B, C, and D exhibited a short lag period but that the early loss by sample A was rapid. After this period, the losses are all linear functions of the square root of the time. The results of a least-squares fit of the data to the equation

$$Q = a + b\sqrt{t}\,, \tag{12}$$

where Q is the amount of leached radioactivity per particle in cpm, and t is the time in minutes, are given in Table 8. Referring to Table 8 and Fig. 8, it appears that the leaching mechanism for sample A was different than that of the other three samples. This result is not understood. For samples B, C, and D, the square-root time dependence indicates a diffusion mechanism. As expected, the leaching rate (b, cpm $\text{min}^{-1/2}$, in Table 8) increases with the particle radius. Also, these three samples showed evidence of etching. The lag period may be attributed to an initially slow attack on the glass surface.

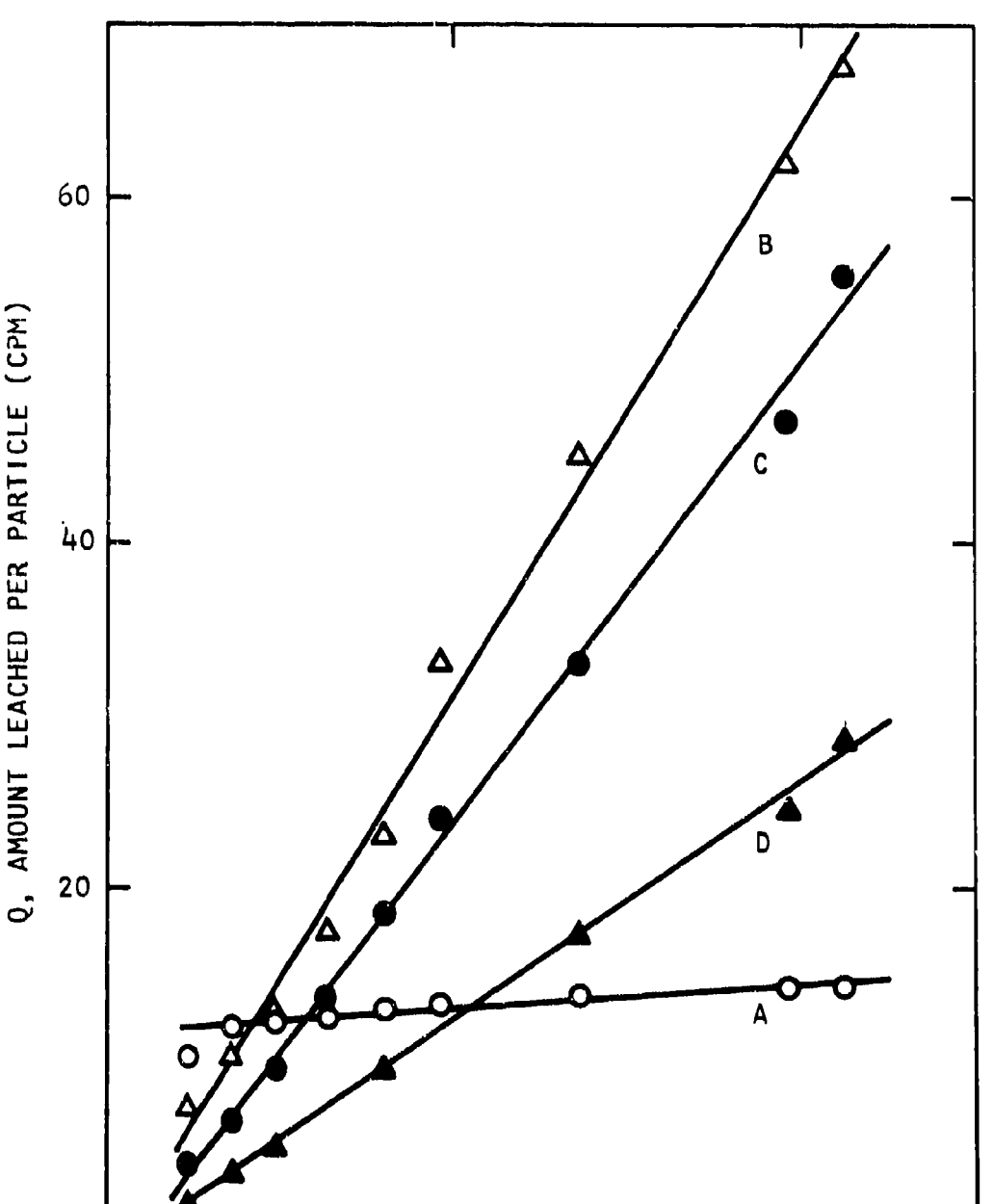

Fig. 8. Leaching of radioactivity from glass spheres by tap water as a function of the square root of the time

TABLE 8

COEFFICIENTS OF EQUATION (12)

a	b	Mean Particle Radius (cm)	b/R^2
11.8	0.0644	0.248	---
-1.69	1.64	0.100	16.4
-2.83	1.33	0.071	26.4
-1.53	0.689	0.052	25.5

The fractional release of the radioactivity by samples B, C, and D may be considered on the basis of diffusion from a sphere with zero surface concentration. Since less than 1% of the activity was lost, this process is described by[16]

$$f = (6/R)\,(Dt/\pi)^{1/2}\,, \qquad (13)$$

where f is the fractional release, R is the radius, D is the diffusion coefficient, and t is the time. Radius-corrected leaching "rates" are presented in the last column of Table 8 as b/R^2. From these data and initial specifications the average value of D that would be associated with the sodium ion was calculated to be 2.2×10^{-11} $cm^2 sec^{-1}$. While it is not certain that sodium ion migration is indeed the rate controlling process, these data certainly suggest this to be the case.

It appears that the leaching of silicates is not a simple phenomenon. In general, the leaching rate depends upon the temperature, the degree of agitation, the pH and nature of the leachant, and the character of the silicate matrix. As an example of the latter, Löcsei[17] studied the leachability of a Na_2O-CaO-MgO-Al_2O_3-SiO_2 system using 10% HCl. The character of the matrices ranged from 100% vitreous to 100% crystalline. His data are described well by an equation of the form

$$S = ae^{-bx}\,, \qquad (14)$$

where S is the solubility ($g/m^2 day$), x is the percentage of crystallinity, and a and b are constants. The effect was pronounced, being roughly two orders of magnitude in S.

In this laboratory further experiments to clarify the leaching problem are in progress. Fission product nuclides are recoiled into flat silicate glass plates that are then sectioned to determine the penetration distribution. Leaching of other recoiled, whole samples is then performed under a variety of experimental conditions. It is expected that the results of these studies with well-defined fission product distributions will make a realistic approach to this part of the fallout problem possible and will result in a leaching model, which, when associated with the cloud chemistry model, will provide a good description of the fission-product biological activity of silicates.

HIGH-TEMPERATURE MASS SPECTROMETRY

RARE-EARTH OXIDE VAPORIZATION STUDIES

A mass spectrometric investigation of the reaction

$$MO_2(g) \rightleftarrows MO(g) + 1/2\ O_2 \qquad (15)$$

for Ce, Pr, and Nd has been completed. Attempts to find other dioxides in the rare-earth series have been unsuccessful, probably due to a temperature limitation of the present apparatus of 2300°K. The work has been written up for submission to the International Journal of Mass Spectrometry and Ion Physics.

Information on Ce was obtained by adding CaO(s) to Ce_2O_3(s) and following the reaction

$$CeO_2(g) + Ca(g) \rightleftarrows CeO(g) + CaO(g) \quad . \qquad (16)$$

Combining this with previously determined data on CaO(g)[18] gave the desired information. Four ΔH measurements were made.

Praseodymium was studied three ways: (1) by using the O_2 gas feed - Ag calibration method, (2) by comparison to the CeO_2-CeO ratio, which was present as an impurity, and (3) by adding CaO. The starting Pr material was a black Pr_xO_y oxide which lost O_2 at about 300°C. The oxide was light green when removed after the experiment; this was probably Pr_2O_3. ΔH was determined four times by (1) and (2), and once by (3).

The O_2 gas feed - Ag calibration method was used for Nd. Light blue Nd_2O_3 was used as the starting material. The sample appeared to be unchanged after the measurements. Four ΔH determinations were made.

Table 9 presents the results obtained for reaction (15).

TABLE 9

RARE-EARTH OXIDE THERMODYNAMICS
(Reaction 15)

Metal	ΔH kcal/mole 2000°K	ΔS eu [a] 2000°K	% 2nd Bond Energy of 1st[19]
Ce	73.5 ± 2.5	18.3 ± 3	72
Pr (1)	39.2 ± 4.6	6.3 ± 3	8
Pr (2)	40.1 ± 1.9	10.8 ± 3	58
Pr (3)	44.7	9.8 ± 3	59
Nd	34.1 ± 5.0	8.3 ± 3	57

[a] Uncertainties were estimated.

The ΔS for the general reaction (15) has been reported by Searcy[20] to be 17 ± 2 eu. This is in good agreement with the Ce data. The Pr and Nd data significantly differ from this and are a cause for concern. Because of this problem, the Pr studies were made in the three mentioned manners. Similar results were obtained as shown in Table 9. Reasons for this difference, if they are not real, can only be suggested. A factor of 100 in the measured equilibrium constant or 15 kcal mole in the ΔH measurement would be needed to achieve agreement between Searcy's estimated ΔS and our measurements. This seems outside our experimental error although a bias in the measured equilibrium constants could conceivably be this big. That is, an anomaly between the efficiency of formation of CeO_2^+ and of PrO_2^+ and NdO_2^+ from neutrals could exist and affect the calibration.

Comparing the second oxygen bond energies from our data with the monoxide bond energies found by White et al.[19] indicates the possibility of more $MO_2(g)$ molecules for the rare earths. Attempts should be made to find them if appropriate apparatus becomes available to handle higher temperature oxidizing systems.

For fallout formation, these studies have shown that the rare earths, which, except for Ce and Pr, were treated as the monoxides in the Henry's

law report,[5] could be generally several orders of magnitude more volatile in a highly oxidizing atmosphere. The rare-earth volatilities probably will be characterized more by the CeO_2 and PrO_2 curves in the Henry's law report than by NdO, PrO, and SmO curves.

RHENIUM AND TECHNETIUM OXYGEN SYSTEMS

A study was initiated to characterize the thermodynamic equilibria involving the gaseous oxides of technetium and oxygen. As a preliminary step in this plan, an investigation of the rhenium-oxygen system was done using two different mass spectrometers and two different furnaces. The mass spectrometers were a Consolidated Electrodynamics Corp. Model 21-703 and an instrument that was partly designed and built at Gulf General Atomic. The former instrument has been described by Norman, Winchell, and Staley,[21] and the latter instrument has been described by Norman and Winchell.[22] The two furnaces and methods of operation were essentially identical except that the background contribution from the furnace region in the Model 21-703 instrument was obtained with a movable cell and a fixed slit, and the background contribution in the other instrument was obtained using a fixed cell and a movable slit. In both cases, the iridium or platinum cells, which contained rhenium metal powder, were provided with oxygen inlet systems. The experiments using the Model 21-703 instrument will be described first.

The temperature was measured with a Pt-Pt/10% Rh thermocouple in contact with the cell base. Temperature gradients were minimized by periodic measurements using an optical pyrometer, followed by power corrections. The important rhenium-containing ions observed were ReO_2^+, ReO_3^+, $HReO_4^+$, $Re_2O_5^+$, $Re_2O_6^+$, and $Re_2O_7^+$. Appearance potential data were in line with the ReO_2^+, $Re_2O_5^+$, and $Re_2O_6^+$ ions being fragment ions. Appearance potentials of the parent ions were ReO_3^+:12.4, $HReO_4^+$:12.6, and Re_2O_7:12.8 eV.

An isothermal O_2 variation experiment was done at 1500°K to clarify the reaction being studied. The results are shown in Fig. 9 where log $(I_{O_2}^+)$ is plotted against $\log(I_{ReO_3}^+)^2/I_{Re_2O_7}^+)$. The experimental slope of ~ - 1/2 indicates that the reaction being studied was

$$Re_2O_7(g) - 2\ ReO_3(g) + 1/2\ O_2(g)\ . \qquad (17)$$

The temperature dependence of reaction (17) was studied with a constant flow of O_2 through the Knudsen cell. Five determinations were made with seven points per determination. The enthalpies were 80.1, 78.0, 74.9, 78.2, and 80.0 kcal mole^{-1} with an average of $\Delta H^\circ_{1500} = 78.2 \pm 2.4$ kcal mole^{-1}, where 1500°K was the approximate midtemperature of the experiments. Figure 10 shows a typical enthalpy determination.

An absolute pressure calibration using silver was done and partial pressures of $O_2(g)$, $ReO_3(g)$, and $Re_2O_7(g)$ were determined using the procedure outlined by Inghram and Drowart.[25] In the calculations, the relative cross sections for ionization by electron impact for O_2 and Ag were taken from Otvos and Stevenson,[24] that for Re was estimated as 50, and those for ReO_3 and Re_2O_7 were obtained from the summation rule.[24] The calibration gave partial pressures at 1487°K of O_2: 3.91×10^{-6}, ReO_3: 1.59×10^{-5}, and Re_2O_7: 2.93×10^{-6} atm. The partial pressures and the enthalpy for reaction (17) yielded a value of $\Delta S^\circ_{1500} = 21.5$ eu for reaction (17).

Similar experiments with the Re-O system were then done using the Gulf General Atomic instrument, the instrument to be used for the technetium studies. The temperature range and O_2 pressures were equivalent to those used in the foregoing experiments. Temperatures were measured using optical pyrometry and care was taken to avoid axial temperature gradients in the platinum Knudsen cell. The mass spectrum and the appearance potentials of the important ions were essentially identical with those found using the Model 21-703 instrument. Using a constant O_2 inlet pressure, three determinations of the temperature dependence of reaction (17) were done yielding

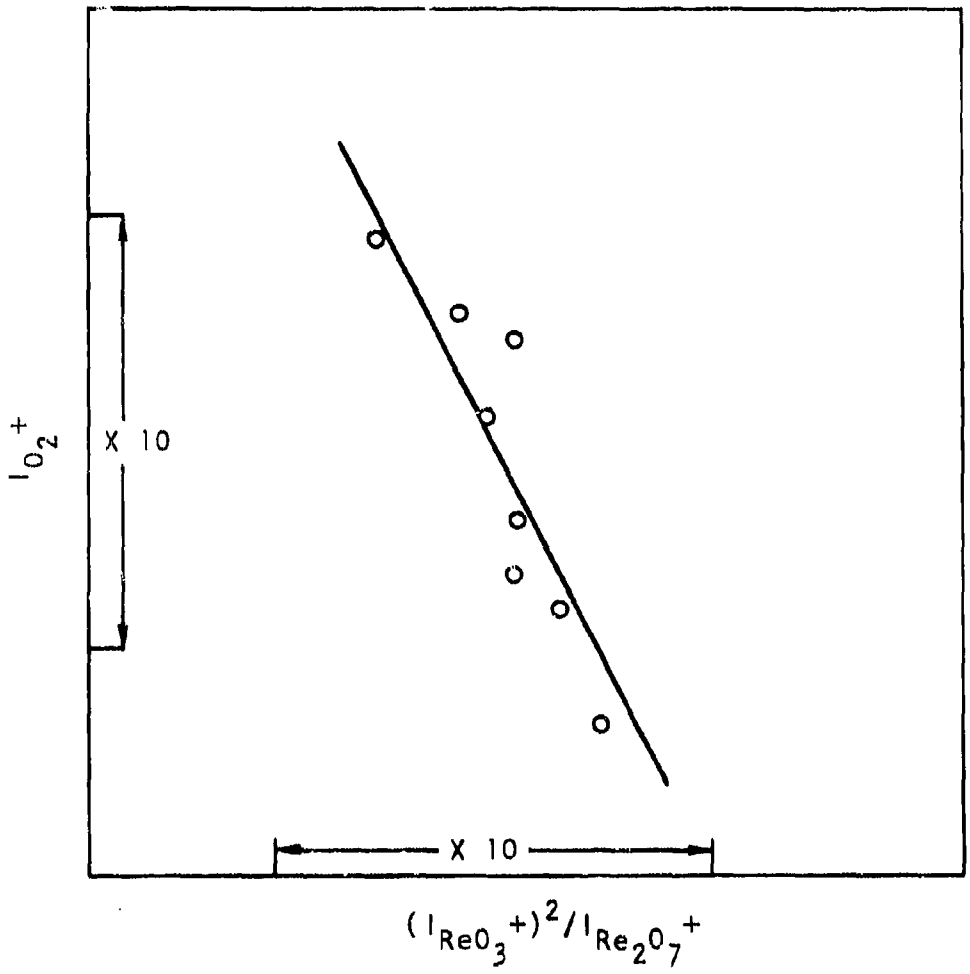

Fig. 9. Results of the O_2 variation experiment. Slope = - 1/2; T = 1500°K

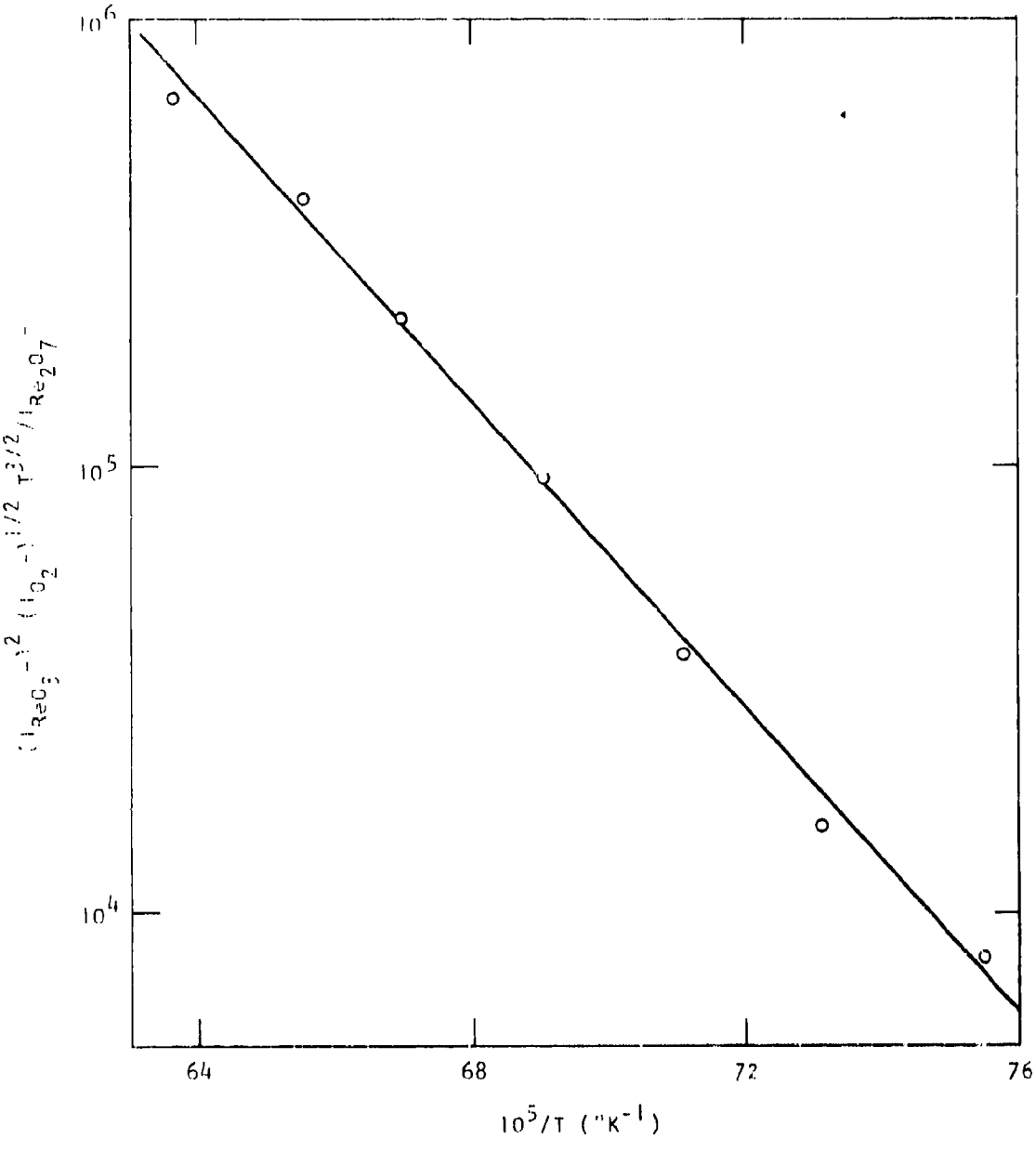

Fig. 10. Typical plot to determine ethalpy for the reaction $Re_2O_7 \rightleftarrows 2ReO_3 + 1/2\ O_2$

an average enthalpy of $\Delta H^{\circ}_{1500} = 108.0 \pm 4.4$ kcal mole^{-1}. Two calibrations of the absolute partial pressures with silver gave a free energy for reaction (17), which was in agreement with that found with the Model 21-703 instrument. However, the average entropy for reaction (17) was found to be $\Delta S^{\circ}_{1500} = 45.2$ eu.

Even considering the uncertainties in the two enthalpy values, there is a large difference between the two entropy values for reaction (17) at 1500°K. The following calculation of the entropy for reaction (17) was made. Using Coughlin's[25] values of the free energy and enthalpy of formation of $Re_2O_7(g)$ at 1500°K with the values of S°_{1500} for Re(s) reported by Stull and Sinke[26] and for $O_2(g)$ given in the JANAF tables,[27] an entropy of $S^{\circ}_{1500} = 172.4$ eu was calculated for $Re_2O_7(g)$. Then, assuming that the JANAF value of S°_{1500} reported for $WO_3(g)$ is similar to that of $ReO_3(g)$, an entropy of $\Delta S^{\circ}_{1500} = 53.9$ eu is found for reaction (17). This value is in fair agreement with the larger experimental value of $\Delta S^{\circ}_{1500} = 45.2$ eu.

Although the higher entropy values for reaction (17) would seem more appropriate, there is strong experimental evidence that the lower value is better. It was stated in the foregoing that the background signals were measured by two distinctly different methods. The contributions to the total ion signal of the species vaporizing from areas adjacent to the cell orifice may be distinguished from the orifice signal with the Model 21-703 instrument. This was not possible with the other instrument. For the Re-O system, the corrections involved were large and temperature-dependent. It is felt that this problem was evinced in the two different enthalpies that were obtained and, hence, in the different entropies.

Although the Tc-O system was expected to present experimental difficulties similar to those found with the Re-O system, a cursory study of the Tc-O system with the Gulf General Atomic instrument was made. Three peaks (not including O_2^+) were observed that could be attributed to neutral gaseous precursors originating in the cell. A mass calibration, which included Hg^+, established the identity of these ions as TcO_3^+, $Tc_2O_5^+$,

and $Tc_2O_7^+$ where the uncertainty of the calibration was ~1 amu. The appearance potentials of these ions, relative to Hg^+, were then measured and their relative intensities were noted. The appearance potential (12.8 eV) and relative intensity of the $Tc_2O_5^+$ ion indicate that this ion could well have as its source a neutral species, $Tc_2O_5(g)$. The Tc-O system would differ from the Re-O system by the presence of $Tc_2O_5(g)$ under conditions where $Re_2O_5(g)$ was not observed. To our knowledge, this is the first mass spectrometric information on the gaseous oxides of technetium. The appearance potentials found for TcO_3^+ (12.2) and $Tc_2O_7^+$ (12.3) are in fair agreement with those for ReO_3^+ (12.4) and $Re_2O_7^+$ (12.8).

Because of the experimental difficulties, it was not possible to make an extensive study of the several equilibrium constants involving oxygen and the technetium oxides. However, the approximate temperature dependences of the three oxides at constant oxygen pressure were measured and these results yielded the intensity ratio data shown in Fig. 11. Using these data, it was possible to calculate the reaction enthalpies, which are listed in Table 10.

TABLE 10

ENTHALPIES FOR GAS-PHASE REACTIONS

1194-1425°K

Reaction	ΔH_T° (kcal/mole)
$Tc_2O_7 + Tc_2O_5 = 4\ TcO_3$	254
$Tc_2O_7 = 2\ TcO_3 + 1/2\ O_2$	136
$Tc_2O_5 + 1/2\ O_2 = 2\ TcO_3$	119
$Tc_2O_7 = Tc_2O_5 + O_2$	17

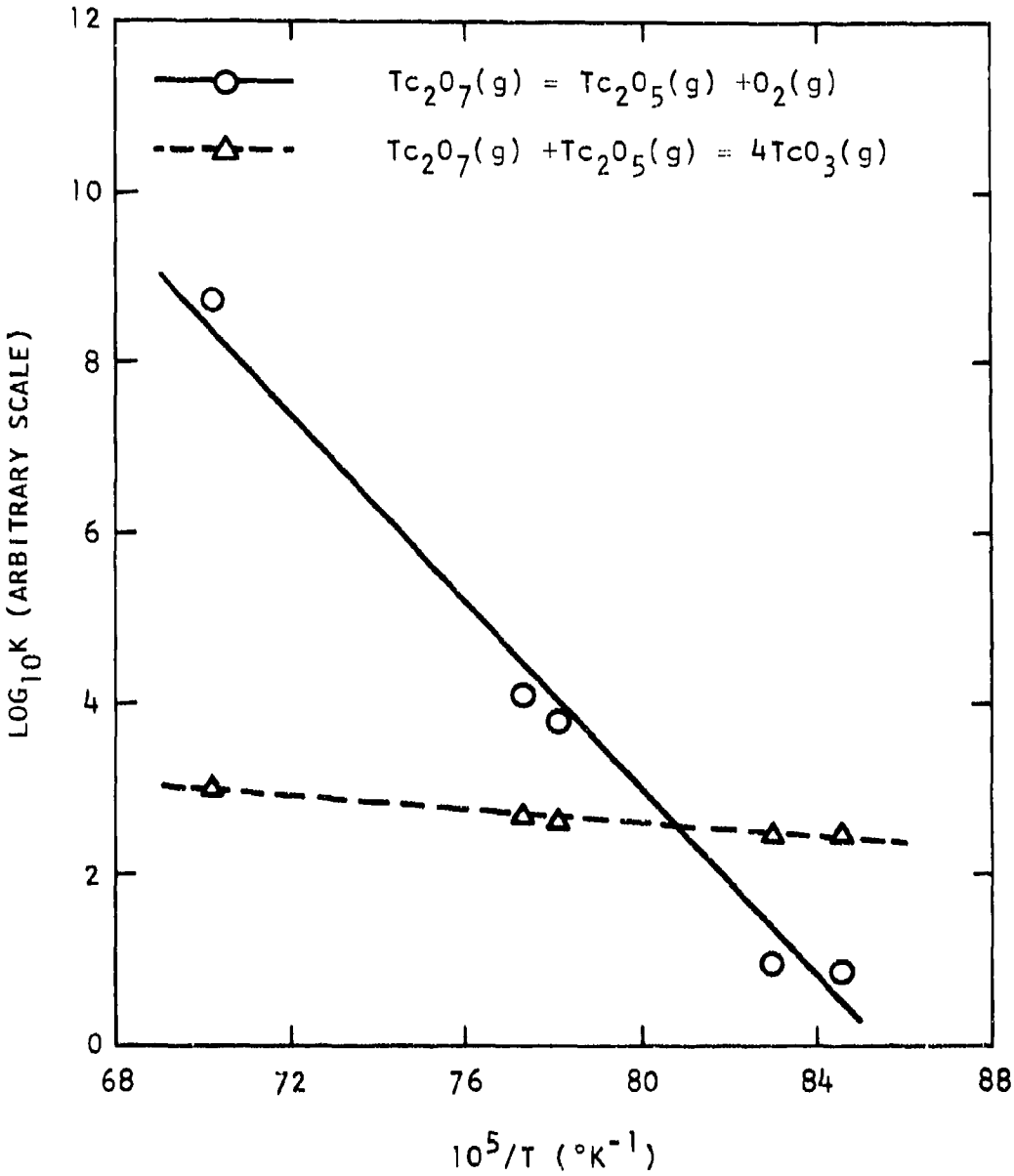

Fig. 11. Equilibrium constant dependence upon temperature for gas-phase reactions between technetium oxides

Although there is a large uncertainty inherent in the enthalpies in Table 10, the values appear to be reasonable. The values for the equilibria involving $Tc_2O_5(g)$ and $Tc_2O_7(g)$ are further evidence for the presence of $Tc_2O_5(g)$, the source of the $Tc_2O_5^+$ ion. However, in a simple, uncontrolled test of oxygen sensitivity the $Tc_2O_5^+$ ion did not respond as would have been expected. It is emphasized that the data leading to these results were derived from a cursory study.

An experiment with the Mn-O system was attempted using the CEC instrument. It was not possible to obtain any data under the experimental conditions used for the Re-O system. However, it was obvious that the Mn-O system is significantly different from the Re-O and Tc-O systems.

REFERENCES

1. Korts, R. F., and J. H. Norman, "A Calculational Model for Condensed State Diffusion Controlled Fission Product Absorption During Fallout Formation," U.S. Naval Radiological Defense Laboratory Report GA-7598, General Dynamics, General Atomic Division, 1967 (AD-651-755).

2. Tompkins, R. C., U.S. Army Nuclear Defense Laboratory, Edgewood Arsenal, Maryland, private communications, 1967.

3. "Department of Defense Land Fallout Prediction System," DASA Technical Operations Research Final Report DASA 1800, v. I through VII, 1966.

4. Freiling, E. C., G. R. Crocker, and C. E. Adams, "Nuclear Debris Formation," Conference on Radioactive Fallout from Nuclear Weapons Tests Proceedings, A. W. Klement, Jr., (ed.), National Bureau of Standards, U.S. Dept. of Commerce, Springfield, Va., 1965, p. 13.

5. Norman, J. H., "Henry's Law Constants for Dissolution of Fission Products in a Silicate Fallout Particle Matrix," U.S. Naval Radiological Defense Laboratory Report GA-7058, General Dynamics, General Atomic Division, 1966 (AD-645-943)

6. Winchell, P., and J. H. Norman, "A Study of the Diffusion of Radioactive Nuclides in Molten Silicates at High Temperatures," Third International Symposium on High Temperature Technology Proceedings, September 17 through 20, 1967, at Asilomar, California, to be published.

7. Miller, C. F., "Fallout and Radiological Countermeasures," v. I., Stanford Research Institute Project No. IM-4021, 1963, p. 26 (AD-410-552).

8. Crocker, G. R., F. K. Kawahara, and E. C. Freiling, "Radiochemical-Data Correlations on Debris from Silicate Bursts," Conference on Radioactive Fallout from Nuclear Weapons Tests Proceedings, A. W. Klement, Jr. (ed.), National Bureau of Standards, U.S. Department of Commerce, Springfield, Va., 1965, p. 72.

9. Freiling, E. C. "Fractionation III Estimation or Degree of Fractionation and Radionuclide Partition for Nuclear Debris," U.S. Naval Radiological Defense Laboratory Report USNRDL-TR-680, 1963.

10. Freiling, E. C., U.S. Naval Radiological Defense Laboratory, San Francisco, private communication, 1967.

11. Norman, J. H., et al., "Henry's Law Constant Measurements for Fission Products Absorbed in Silicates," IAEA Symposium on Thermodynamics of Nuclear Materials with Emphasis on Solution Systems Proceedings, September 4 through 8, 1967, Vienna, to be published.

12. Merten, U., J. Phys. Chem. 63, 443 (1959).

13. Norman, J. H., and P. Winchell, "Cloud Chemistry of Fallout Formation, Final Report," General Dynamics, General Atomic Division Report GA-7597, 1967.

14. Yang, L., and M. T. Simnad, "Measurement of Diffusivity in Liquid Systems," in Physicochemical Measurements at High Temperatures, Academic Press, Inc., New York, 1959, p. 304.

15. Gordon, G. E., J. W. Harvey, and H. Nakahara, Nucleonics 24, 62 (1966).

16. Crank, J., The Mathematics of Diffusion, Oxford University Press, London, 1956, p. 87.

17. Löcsei, B. P., "Acid Resistance of Vitroceramic Materials on a Feldspar-Diopside Base," in Symposium on Nucleation and Crystallization in Glasses and Melts, The American Ceramic Society, Inc., Columbus, 1962, p. 71.

18. Norman, J. H., et al., "Fallout Studies, Cloud Chemistry, Final Report," Office of Civil Defense Report GA-6094, General Dynamics, General Atomic Division, 1965 (AD-614-997).

19. White, D., et al., IAEA Symposium on Thermodynamics of Nuclear Materials Proceedings, May 21 through 25, 1962, Vienna, p. 417.

20. Searcy, A. W., "High-Temperature Reactions," in Survey of Progress in Chemistry I, Academic Press, Inc., New York, 1963, p. 35.

21. Norman, J. H., P. Winchell, and H. G. Staley, J. Chem. Phys. 41, 60 (1964).

22. Norman, J. H., and P. Winchell, J. Phys. Chem. 68, 3802 (1964).

23. Inghram, M. G., and J. Drowart, "Mass Spectrometry Applied to High Temperature Chemistry," in Proceedings of an International Symposium on High Temperature Technology, McGraw-Hill Book Co., Inc., New York, 1960, p. 219.

24. Otvos, J. W., and D. P. Stevenson, J. Am. Chem. Soc. 78, 546 (1956).

25. Coughlin, J. P., "Contributions to the Data on Theoretical Metallurgy XII, Heats and Free Energies of Formation of Inorganic Oxides," Bulletin 452, U.S. Bureau of Mines, Washington, 1954.

26. Stull, D. R., and G. C. Sinke, Thermodynamic Properties of the Elements, American Chemical Society, Washington, 1956.

27. Joint Army, Navy, and Air Force Thermochemical Tables, The Dow Chemical Company, Midland, Michigan, 1965.

DISTRIBUTION LIST

(One copy each unless indicated otherwise.)

Office of Civil Defense
Office of Secretary of Army
Attn: Director for Research
The Pentagon
Washington, D.C. 20310
(Remainder)

Department of Sanitary Engineering
Walter Reed Army Institute of Research
Washington, D.C. 20012

COL Jack Redmond
Office of the Surgeon General
Main Navy Building
Washington, D.C. 20360

Commanding General
Combat Developments Command
Materiel Requirements Division
Fort Belvoir, Virginia 22060

Defense Logistics Studies Information Exchange
U.S. Army Logistics Management Center

Fort Lee, Virginia 23801
(2 copies)

Assistant Secretary of the Army (R&D)
Attn: Assistant For Research
Washington, D.C. 20310

Army Library, TAGO
Civil Defense Unit
Room 1A518
The Pentagon
Washington, D.C. 20310
(3 copies)

Dr. E.E. Massey
Defense Research Board
Ottawa, Canada

Mr. Paul Zigman, Code 908
Head, Technical Management
U.S. Naval Radiological Defense Laboratory
San Francisco, California 94135
(10 copies)

Chief of Naval Research (Code 104)
Department of the Navy
Washington, D.C. 20360

Chief of Naval Operations (Op-07T10)
Department of the Navy
Washington, D.C. 20350

The Engineer School
Attn: Library
Fort Belvoir, Virginia 22060

U.S. Army Engineer Research and Development Laboratories
Attn: Technical Library
Fort Belvoir, Virginia 22060

Joint Civil Defense Support Group
Office of the Chief of Engineers
Department of the Army
Gravelly Point, Virginia 20315

Army Nuclear Defense Laboratory
Attn: Technical Library
Edgewood, Maryland 21010

U.S. Naval Civil Engineering Laboratory
Attn: Library
Port Hueneme, California 93041

Strategic Planning Group (Code 9001)
U.S. Army Map Service
Attn: Vulnerability Analysis
Washington, D.C. 20315

Assistant Secretary of the Air
Force (R&D)
Room 4E968
The Pentagon
Washington, D. C. 20330

COL Converse Lewis
Medical Field Service School
Department of Preventive Medicine
Fort Sam Houston, Texas 78200

Dr. Harold Knapp
Weapons Systems Evaluation Division
Institute for Defense Analysis
400 Army Navy Drive
Arlington, Virginia 22202

Advanced Research Projects Agency
Department of Defense
The Pentagon
Washington, D. C. 20301

Defense Documentation Center
Cameron Station
Alexandria, Virginia 22314
(20 copies)

U. S. Atomic Energy Commission
Hq., Reports Library, G-017
Germantown, Maryland 20545

The RAND Corporation
Attn: H. H. Mitchell, M. D.
Santa Monica, California 90406

U. S. Atomic Energy Commission
Technical Information Service
Oak Ridge, Tennessee 37830

Dr. Walter Wood
Dikewood Corporation
1009 Bradbury Drive, S. E.
University Research Park
Albuquerque, New Mexico 87106

Dr. Herman Kahn
Hudson Institute
Quaker Ridge Road
Harmon-on-Hudson, New York 10520

Dr. Eugene Sevin
IIT Research Institute
10 West 35th Street
Chicago, Illinois 60616

Institute for Defense Analysis
Attn: Dr. Abner Sachs
400 Army Navy Drive
Arlington, Virginia 22202

NASA Headquarters
Office of Advanced Research and
Technology
1512 H Street, N. W.
Washington, D. C. 20546

Advisory Committee on Civil Defense
National Academy of Sciences
2101 Constitution Avenue, N. W.
Attn: Mr. Richard Park
Washington, D. C. 20418

Dr. Stanley Auerbach
Radiation Ecology Section
Health Physics Division
Oak Ridge National Laboratory
Oak Ridge, Tennessee 37831

Dr. Eugene P. Wigner
Oak Ridge National Laboratory
Oak Ridge, Tennessee 37831

Dr. Joseph Coker
Office of Emergency Planning
Washington, D. C. 20504

Division of Health Mobilization
Public Health Service
Department of Health, Education
and Welfare
Washington, D.C. 20202

U.S. Office of Education
Department of Health, Education
and Welfare
Attn: Director, Civil Defense
Adult Education Staff
Washington, D.C. 20202

Dr. Edgar Parsons
Research Triangle Institute
P.O. Box 490
Durham, North Carolina 27702

Mr. William White
Stanford Research Institute
Menlo Park, California 94025
(3 copies)

Dr. Carl F. Miller
Stanford Research Institute
Menlo Park, California 94025

Dr. Eric Clarke
Technical Operations Research
Burlington, Massachusetts 01338

Mr. Myron B. Hawkins
United Research Services
1811 Trousdale Avenue
Burlingame, California 94011

Water and Sewage Industry and
Utilities Division
U.S. Department of Commerce
Washington, D.C. 20230

Defense Atomic Support Agency
Attn: Library
The Pentagon
Washington, D.C. 20301

Defense Atomic Support Agency
Commander Field Command
Sandia Base
Albuquerque, New Mexico 87100

Defense Communications Agency
8th & South Courthouse Road
Arlington, Virginia 22204

Defense Intelligence Agency
(DIAAP-1K2)
Washington, D.C. 20301

Chief, NMCSSC
The Pentagon, Room EE685
Washington, D.C. 20301

Army War College
Attn: Library
Fort McNair, Washington, D.C.

Civil Defense Research Project
Oak Ridge National Laboratory
P.O. Box X
Oak Ridge, Tennessee 37830

Air University
Attn: Library
Maxwell Air Force Base, Alabama
26052

U.S. Air Force Special
Weapons Center
Kirtland Air Force Base
Attn: Library
Albuquerque, New Mexico 87417

Mr. Ed. Saunders
Research Division
Office of Emergency Planning
Washington, D.C. 20504

Dr. Bernard Shore
University of California
Lawrence Radiation Laboratory
P.O. Box 808
Livermore, California 94550

Civil Defense Technical Services Center
College of Engineering
Department of Engineering
Gainesville, Florida 32601

Director
Disaster and Defense Services Staff
Agricultural Stabilization and
Conservation Service
U.S. Department of Agriculture
Washington, D.C. 20250

Commanding Officer
U.S. Army Nuclear Defense Laboratory
Attn: Mr. Harry Bouton
Army Chemical Center
Edgewood, Maryland 21010

LT COL David W. Duttweiler
Hw., Medical R&D Command
Main Navy Building
Washington, D.C. 20360

Chief, Bureau of Ships (Code 203)
Department of the Navy
Washington, D.C. 20360

Chief, Bureau of Ships (Code 335)
Department of the Navy
Washington, D.C. 20360
(2 copies)

CDR W.J. Christensen
U.S. Naval Civil Engineering Laboratory
Port Hueneme, California 93041

Dr. Josh Holland
Division of Biology and Medicine
U.S. Atomic Energy Commission
Washington, D.C. 20545

Dr. John Wolfe
U.S. Atomic Energy Commission
Washington, D.C. 20545

Dr. Arnold H. Sparrow
Biology Department
Brookhaven National Laboratory
Upton, Long Island, New York 11973

Dr. A.B. Park
Agricultural Research
U.S. Department of Agriculture
Washington, D.C. 20250

Mr. Harvey Ludwig
Engineering Science Inc.
150 East Foothills Blvd.
Arcadia, California 91006

Dr. John Norman
General Dynamics Corporation
P.O. Box 5
Old San Diego Station
San Diego, California 92112

Dr. Leo K. Bustad
University of California
Davis, California 95616

Dr. Werner N. Grune
Professor of Civil Engineering
Merrimack College
North Andover, Massachusetts 01060

Dr. Morgan Seal
U.S. Public Health Service
P.O. Box 684
Las Vegas, Nevada 89100

Mr. James G. Terrell, Jr.
Radiological Health Division
U.S. Public Health Service, DHEW
Washington, D.C. 20201

Dr. Kermit Larson
Atmospheric Physics Research Section
Battelle, N.W.
2704 W. Bldg., 200 W. Area
Richland, Washington 99352

Dr. John R. Rust
Section of Nuclear Medicine
University of Chicago
947 E. 58th Street
Chicago, Illinois 60600

Commanding General
U. S. Army Electronics Command
Attn: AMSEL-BL-MA
Mr. Conover
Fort Monmouth, New Jersey 07703

Air Force Weapons Laboratory
(WLRB)
Kirtland Air Force Base, New Mexico

Commanding Officer
U. S. Army Combat Developments
Command
Attn: Effects Div. (MAJ Delamain)
Nuclear Group
Fort Bliss, Texas 79916

Commanding Officer
U. S. Army Combat Developments
Command
Attn: Mr. Whitten
CBR Agency
Fort McClellan, Alabama 36201

Project Supervisor, Marvin Polan
Ford Instrument Company
31-01 Thomson Avenue
Long Island City, New York 11100

Mr. Bill Miller
Dept. of Civil Engineering
307 More Hall
University of Washington
Seattle, Washington 98100

Mr. Carl Koontz
Department of Civil Engineering
Worcester Polytechnic Institute
Worcester, Massachusetts 01600

Franklin J. Agardy
Department of Civil Engineering
San Jose State College
San Jose, California 95100

M. B. Scott
School of Civil Engineering
Civil Engineering Building
Purdue University
Lafayette, Indiana 47901

Charles H. Samson, Jr.
Head, Civil Engineering Dept.
Texas A&M University
College Station, Texas 77840

Dr. Harold Brode
Rand Corporation
Santa Monica, California 90406

Ottawa University
Department of Physics
Attn: Dr. L.V. Spencer
Ottawa, Kansas 66067

University of Illinois
Department of Civil Engineering
Attn: Prof. A.B. Chilton
Urbana, Illinois 61803

Mr. Charles Eisenhauer
National Bureau of Standards
Radiation Theory Section 4.3
Washington, D.C. 20324

Kansas State University
Department of Nuclear Engineering
Attn: Dr. W. Kimel
Manhattan, Kansas 66504

Chemical Laboratories
Defense Research Board
Attn: Dr. C.E. Clifford
Ottawa, Canada

Edgerton, Germeshausen & Grier, Inc.
P.O. Box 1912
Attn: Mr. Z.G. Burson
Las Vegas, Nevada 89100

Director
Oak Ridge National Laboratory
P.O. Box X
Attn: Dr. J. Auxier
Oak Ridge, Tennessee 37831

Director
Oak Ridge National Laboratory
P.O. Box X
Attn: Mr. C.E. Clifford
Oak Ridge, Tennessee 37831

Dr. Cyril L. Comar
Cornell University
New York State University
Department of Physical Biology
Ithaca, New York 14850

Dr. Harvey L. Cromroy
Department of Radiation Biology
University of Florida
Gainesville, Florida 32601

Dr. Roy Overstreet
Department of Soils and Plant Nutrition
University of California
Berkeley, California 94700

UNCLASSIFIED
Security Classification

DOCUMENT CONTROL DATA - R & D

(Security classification of title, body of abstract and indexing annotation must be entered when the overall report is classified)

1. ORIGINATING ACTIVITY (Corporate author)
Gulf General Atomic Incorporated
San Diego, California

2a. REPORT SECURITY CLASSIFICATION
Unclassified

2b. GROUP

3. REPORT TITLE
Cloud Chemistry of Fallout Formation
Final Report

4. DESCRIPTIVE NOTES (Type of report and inclusive dates)

5. AUTHOR(S) (First name, middle initial, last name)
John H. Norman, Perrin Winchell, and Harry G. Staley

6. REPORT DATE	7a. TOTAL NO. OF PAGES	7b. NO. OF REFS
January 31, 1968	48	27

8a. CONTRACT OR GRANT NO	9a. ORIGINATOR'S REPORT NUMBER(S)
N0022867C1675	GA-8472
b. PROJECT NO	
c.	9b. OTHER REPORT NO(S) (Any other numbers that may be assigned this report)
d.	

10. DISTRIBUTION STATEMENT
Each transmittal of this document outside agencies of the U.S. Government must have prior approval of the Office of Civil Defense, Office of Secretary of Army.

11. SUPPLEMENTARY NOTES	12. SPONSORING MILITARY ACTIVITY
	Office of the Civil Defense Office of the Secreatry of the Army Washington, D.C. 20310

13. ABSTRACT

Calculations of fission-product distribution in fallout for the Small Boy event have been made using a condensed-state diffusion-controlled fission-product absorption model. The properties of calculated fission-product inventories in particles with size distribution supplied correlated reasonably well with properties of actual Small Boy fallout inventories. An evaluation of these inventories using the DELFIC fission-product distribution system is being made.

Henry's law has been demonstrated to be applicable to the system cesium/O_2/CaO-Al_2O_3-SiO_2 eutectic. The derived Henry's law constants have been shown to be independent of the oxygen pressure ($1 \geq P_{O_2}$ (atm) $> \sim 10^{-4}$) and of water pressure ($0.03 \geq P_{H_2O}$ (atm) $> \sim 10^{-4}$).

The diffusion coefficients of cesium in Small Boy soil have been measured. These measurements provide some justification for employing diffusion coefficients of fission products in CaO-Al_2O_3-SiO_2 eutectic for the Small Boy calculations. Studies of diffusion coefficients of fission products created in situ in silicate matrices have been initiated.

Some preliminary fission-product leaching studies have been made. A program for studying the leaching of recoiled fission products from silicates is outlined.

Mass spectrometric Knudsen cell studies have demonstrated the apparent importance of such species as $CeO_2(g)$, $PrO_2(g)$, $NdO_2(g)$, and $TcO_3(g)$ to fallout formation processes.

DD FORM 1 NOV 68 1473

UNCLASSIFIED
Security Classification

14. KEY WORDS	LINK A		LINK B		LINK C	
	ROLE	WT	ROLE	WT	ROLE	WT
Henry's Law Constants						
Fission Product Absorption						
Diffusion Studies						
Fallout Formation						
Cloud Chemistry						
Leaching Studies						
High-Temperature Mass Spectrometry						
Knudsen Cell Studies						
Transpiration Studies						